presented at 2024 5th Information Communication Technologies Conference (ICTC) (DOI: 10.1109/ICTC61510.2024.10601808)

# Local Subdivisional Channel Estimation in RIS-Assisted THz MIMO-OFDM Systems

Yifang Dai, Wuqiong Zhao, You You, Yongming Huang, and Chuan Zhang*
[1]Lab of Efficient Architectures for Digital-communication and Signal-processing (LEADS),
National Mobile Communications Research Laboratory, Southeast University, Nanjing, China
[2]Purple Mountain Laboratories, Nanjing, China
Email: chzhang@seu.edu.cn

***Abstract*—Reconfigurable intelligent surfaces (RIS) offer significant performance gains for terahertz (THz) multiple-input and multiple-output (MIMO)-orthogonal frequency division multiplexing (OFDM) systems. However, channel estimation (CE) in high-dimensional RIS channels remains challenging. This paper proposes a compressed sensing (CS)-based CE method that separates angle and gain estimation, reducing pilot overhead and computational complexity. We leverage spatial path selection enabled by designed beam and reflection patterns to reduce dimensionality. Our method achieves over 35% pilot overhead reduction and significantly improves computational efficiency, while maintaining accuracy comparable to existing methods.**

***Index Terms*—Reconfigurable intelligent surface (RIS), channel estimation (CE), compressed sensing (CS), terahertz (THz).**

## I. Introduction

Terahertz (THz) communication, leveraging its vast bandwidth, enables high data transmission rates in 6G [1]. However, the characteristics of high directionality and substantial path loss restrict its optimal performance to line-of-sight links [2]. The reconfigurable intelligent surface (RIS), capable of transforming wireless communication channels, has garnered significant attention in THz multiple-input multiple-output (MIMO) systems [3] to mitigate these challenges. Nonetheless, the large number of passive elements in the RIS and the wide bandwidth characteristics of THz channels complicate channel estimation (CE) and result in extremely large pilot overhead.

In recent years, compressed sensing (CS)-based CE methods have been explored to reduce pilot overhead while achieving satisfactory estimation performance. Orthogonal matching pursuit (OMP) [4] and OMP list (OMPL) [5] have been proposed for efficient CE using CS in millimeter wave (mmWave) MIMO systems considering the angle-domain sparsity. A three-stage split estimation method [6], a novel cascaded CE formula that splits the angle-domain grid of RIS [7], and a Bayesian learning CE method [8] have also been developed. Additionally, the impact of delay on the accuracy of THz wideband CE has been discussed in [9], and pilot overhead has been reduced by extrapolating the subchannels activated by a subset of RIS elements to the complete channel [10]. The OMPL-SBL algorithm [11], balancing complexity and accuracy in RIS-assisted mmWave MIMO systems, considers the grid sparsity structure in the angle domain.

However, in orthogonal frequency division multiplexing (OFDM) systems, the large number of subcarriers makes the overhead of pilot signals and complexity difficult to sustain. To address this challenge, a block sparse channel model amenable to estimation via block orthogonal matching pursuit (BOMP) has been proposed by utilizing the fact that different subcarriers share the same support [12]. However, the constructed block sparse channel vector has a large dimension, maintaining a high computational complexity. Notably, the wideband beam squint effect is not considered in this paper as it can be effectively alleviated by subcarrier grouping [13]. Besides, the generalized simultaneous orthogonal matching pursuit (G-SOMP) algorithm [14] leverages information from multiple subcarriers, effectively restoring subcarrier channels.

This paper proposes a local subdivisional CE method with high temporal efficiency for THz MIMO-OFDM systems. By prioritizing the estimation of angles for each path, followed by estimating path gains and delays based on angle information, we significantly reduce complexity and pilot overhead. The key contributions are summarized as follows:

1) RIS reflection patterns are designed for CS-based CE in THz MIMO-OFDM systems, reducing pilot overhead and complexity while improving accuracy;
2) The proposed three-stage method introduces spatial path selection to reduce dimensions, with separate angle estimation and gain estimation stages;
3) By leveraging path-wise estimation to mitigate the wideband effect, the proposed method achieves higher pilot efficiency through a designed RIS switching scheme.

## II. System Model

This paper investigates a single-user THz MIMO system aided by RIS. Both the user equipment (UE) and base station (BS) are equipped with $N_t$ and $N_r$ antennas, arranged in uniform linear arrays (ULAs). To address the challenge of high path loss in terahertz channels, the RIS is deployed near the BS [15]. The $b$-th subcarrier of the uplink cascaded channel in an OFDM system with bandwidth $B$ and center frequency $f_c$ can be expressed as

$$\mathbf{H}[b] = \mathbf{H}_G[b]\,\mathrm{diag}(\mathbf{\Phi})\mathbf{H}_R[b], \tag{1}$$

where $\mathrm{diag}(\mathbf{\Phi})$ denotes the diagonal matrix of vector $\mathbf{\Phi}$, and $\mathbf{\Phi} \in \mathbb{C}^{M\times 1}$ represents the reflection vector of the RIS which is an $M = M_x \times M_y$ uniform planar array (UPA). The BS–RIS channel $\mathbf{H}_G$ and the UE–BS channel $\mathbf{H}_R$ utilize

a wideband geometric channel model [12]. Specifically, the RIS–BS channel for the $b$-th subcarrier can be represented as

$$\mathbf{H}_G[b] = \sum_{p_1=1}^{P_1} \alpha_{p_1,b} \mathbf{a}_{B,b}\left(\phi_{p_1}\right) \mathbf{a}_{R,b}\left(\vartheta_{p_1}^t, \varphi_{p_1}^t\right)^{\mathsf{H}} e^{-j2\pi\tau_{p_1} f_b}, \quad (2)$$

where $(\cdot)^{\mathsf{H}}$ denotes the conjugate transpose. Here, $P_1$ is the number of RIS–BS paths, $\mathbf{a}_{B,b}\left(\phi_{p_1}\right)$ and $\mathbf{a}_{R,b}\left(\vartheta_{p_1}^t, \varphi_{p_1}^t\right)$ detailed in [12] respectively represent the BS and RIS array response vectors, while $\phi_{p_1}$, $\vartheta_{p_1}^t$, and $\varphi_{p_1}^t$ represent the arrival angle at the BS and the departure azimuth and elevation angles at the RIS. Additionally, $\tau_{p_1}$ denotes the channel delay of the $p_1$-th path and $f_b$ represents the frequency of the $b$-th subcarrier. Similar to Eq. (2), the UE–RIS channel $\mathbf{H}_R$ has

$$\mathbf{H}_R[b] = \sum_{p_2=1}^{P_2} \alpha_{p_2,b} \mathbf{a}_{R,b}\left(\vartheta_{p_2}^r, \varphi_{p_2}^r\right) \mathbf{a}_{u,b}(\Phi_{l_2})^{\mathsf{H}} e^{-j2\pi\tau_{p_2} f_b}, \quad (3)$$

where $P_2$ is the number of UE–RIS paths while $\vartheta_{p_2}^r$, $\varphi_{p_2}^r$ and $\Phi_{l_2}$ respectively represent the azimuth and elevation angles of arrival at the RIS, and the departure angle at the UE. $\mathbf{a}_{u,b}(\Phi_{l_2})$ is the UE array response vector.

The extremely sparse nature of terahertz channels encourages the adoption of spatial dictionaries in the angle domain to construct a sparse virtual representation [7]. Consequently, $\mathbf{H}_G[b]$ and $\mathbf{H}_R[b]$ can be decomposed as

$$\begin{cases} \mathbf{H}_G[b] = \mathbf{D}_B[b]\widetilde{\mathbf{\Omega}}_G[b]\mathbf{D}_R^{\mathsf{H}}[b], \\ \mathbf{H}_R[b] = \mathbf{D}_R[b]\widetilde{\mathbf{\Omega}}_R[b]\mathbf{D}_u^{\mathsf{H}}[b], \end{cases} \quad (4)$$

where $\mathbf{D}_B[b] \in \mathbb{C}^{N_r \times N_r^D}$, $\mathbf{D}_R[b] \in \mathbb{C}^{M \times M^D}$ and $\mathbf{D}_u[b] \in \mathbb{C}^{N_t \times N_t^D}$ respectively represent the angle-domain spatial grid dictionaries at the BS, RIS and UE, containing $N_r^D$, $M^D$ and $N_t^D$ array response vectors. $\widetilde{\mathbf{\Omega}}_G[b]$ and $\widetilde{\mathbf{\Omega}}_R[b]$ represent the sparse RIS–BS and UE–RIS angle domain channel matrices with $P_1$ and $P_2$ non-zero elements, respectively. Given the beamforming precoding matrix $\mathbf{F}$ and combining matrix $\mathbf{W}$ as described in [7], the received signal for the $b$-th subcarrier corresponding to the $k$-th reflection pattern is expressed as

$$\mathbf{Y}_k[b] = \mathbf{W}^{\mathsf{H}}\mathbf{H}_G[b]\,\mathrm{diag}(\mathbf{\Phi}_k)\mathbf{H}_R[b]\mathbf{F} + \mathbf{N}_k[b], \quad (5)$$

where $\mathbf{Y}_k[b] \in \mathbb{C}^{N_t^B \times N_r^B}$ is the received signal with $N_t^B$ transmit beams at the UE and $N_r^B$ receive beams at the BS, respectively. Reviewing channel decomposition in Eq. (4) and following the channel transformation conducted in [7], Eq. (5) can be transformed as

$$\mathbf{y}_k[b] = \left((\widetilde{\mathbf{C}}_R[b]\mathbf{\Phi}_k)^{\mathsf{T}} \otimes \mathbf{P}(\mathbf{D}_u^*[b] \otimes \mathbf{D}_B[b])\right)\mathbf{s}_k[b] + \mathbf{n}_k[b], \quad (6)$$

where $(\cdot)^{\mathsf{T}}$ denotes the transpose, $(\cdot)^*$ denotes the conjugate and $\otimes$ represents the Kronecker product. $\mathbf{P} \triangleq \mathbf{F}^{\mathsf{T}} \otimes \mathbf{W}^{\mathsf{H}}$ represents the precoding component, and $\widetilde{\mathbf{C}}_R[b] \triangleq (\mathbf{D}_R^{\mathsf{T}}[b] \circledcirc \mathbf{D}_R^{\mathsf{H}}[b])(:, 1 : M^D)$ denotes the compressed RIS angle-domain spatial dictionary matrix, as described in [16], with $\circledcirc$ representing the Khatri–Rao product. Additionally, $\mathbf{s}[b] \in \mathbb{C}^{N_r^D N_t^D M^D}$ is a sparse vector. Following [7], Eq. (6) is transformed into

$$\mathbf{y}_k[b] = \mathbf{P}(\mathbf{D}_u^*[b] \otimes \mathbf{D}_B[b])\boldsymbol{\omega}_k[b] + \mathbf{n}_k[b], \quad (7)$$

where $\boldsymbol{\omega}_k[b]$ represents the combined sparse vector, which according to [7] satisfies

$$\boldsymbol{\omega}_k[b] = \sum_{n=1}^{N} [\widetilde{\mathbf{C}}_R[b]\mathbf{\Phi}_k]_n \mathbf{s}_n[b], \quad (8)$$

where $[\widetilde{\mathbf{C}}_R[b]\mathbf{\Phi}_k]_n$ is the $n$-th element of vector $\widetilde{\mathbf{C}}_R[b]\mathbf{\Phi}_k$. $n$ represents the indices of non-zero elements in $\widetilde{\mathbf{C}}_R[b]\mathbf{\Phi}_k$ and $\mathbf{s}_n[b] \triangleq \mathbf{s}[b]\left((n-1)N_r^D N_t^D + 1 : nN_r^D N_t^D\right)$. For $\widetilde{\mathbf{C}}_R[b]\mathbf{\Phi}_k$, each element represents the influence of the corresponding angle-domain grid on the RIS for the specific paths, achieving spatial path selection. Consequently, when an element in $\widetilde{\mathbf{C}}_R[b]\mathbf{\Phi}_k$ is zero, it indicates that the path corresponding to the angle at the RIS is obstructed and unable to reach the BS.

## III. Proposed Method

The overall framework of our proposed method is illustrated in Fig. 1, where we initially perform spatial path selection to obtain angle and delay information at the RIS, then design corresponding RIS reflection patterns for path-wise estimation to acquire angle information at the UE and BS, and finally, we collectively obtain the path gains for all subcarriers.

### A. Angle and Delay Estimation at RIS

This stage acquires angle and path delay information at the RIS for subsequent CE, using specific subcarriers to minimize overhead. The challenge is obtaining RIS angle-domain information with minimal pilots. A general approach exhaustively searches the RIS angle domain with $K = M^D$ reflection patterns [7], ensuring one non-zero element in $\widetilde{\mathbf{C}}_R[b]\mathbf{\Phi}_k$ for $M^D$ angle-domain grids. However, THz channel sparsity results in fewer paths, making this approach inefficient. Exploiting RIS angle domain sparsity, we design reflection patterns $\mathbf{\Phi}_{k_1}$ (Eq. (9)) to construct partially sparse $\widetilde{\mathbf{C}}_R[b]\mathbf{\Phi}_{k_1}$, enabling region-based retrieval and spatial path selection:

$$\mathbf{\Phi}_{k_1} = \mathbf{F}(:, k_1), \quad (9)$$

where $\mathbf{F}(:, k_1)$ is the $k_1$-th column of of the discrete Fourier transform (DFT) matrix $\mathbf{F} \in \mathbb{C}^{M \times M}$, and $k_1 = 1, 2, \ldots, M_x^D - 1$. With the design in Eq. (9), each $\widetilde{\mathbf{C}}_R[b]\mathbf{\Phi}_{k_1}$ is partially sparse, with only $M_y^D$ non-zero elements. Hence, by detecting received signals at the receiver, we can obtain the path region information $\mathbf{r}$ where the RIS angle is located as

$$\mathbf{r} = \{k_1 \mid \|\mathbf{y}_{k_1}[b]\|_2 > \varepsilon_0\}, \quad (10)$$

where $\mathbf{y}_{k_1}[b]$ is the received signal using reflection pattern $\mathbf{\Phi}_{k_1}$ for the $b$-th subcarrier, and $\varepsilon_0$ is a small threshold. Based on $\mathbf{r}$, we retrieve angles within existing path regions by scanning angle grids using the reflection pattern:

$$\mathbf{\Phi}_{\widetilde{k}_1,r} = \frac{M^D}{M}\widetilde{\mathbf{C}}_R^{\dagger}[b](:, M_x^D[\mathbf{r}]_r + \widetilde{k}_1), \quad (11)$$

where $\widetilde{\mathbf{C}}_R^{\dagger}[b]$ is the pseudo-inverse of $\widetilde{\mathbf{C}}_R[b]$, $r = 1, 2, \ldots, R$, and $R$ is the number of predefined regions. $\mathbf{\Phi}_{\widetilde{k}_1,r}$ is the $\widetilde{k}_1$-th reflection pattern used for secondary scanning in each

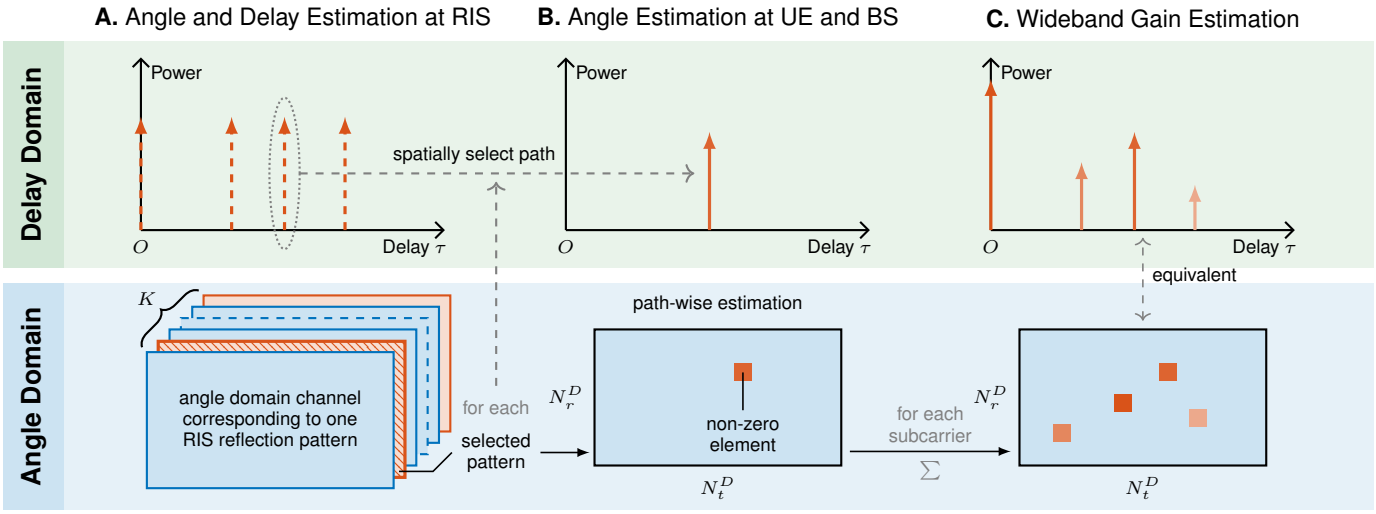


Fig. 1. The proposed scheme decomposes the wideband cascaded CE into 'angle and delay estimation at RIS,' 'angle estimation ar UE and BS,' and 'wideband gain estimation.'

predefined region. The RIS angle information $\mathbf{i}_R$ is then obtained as

$$\mathbf{i}_R = \{M_x^D[\mathbf{r}]_r + \widetilde{k}_1 \mid \|\mathbf{y}_{\widetilde{k}_1,r}[b]\|_2 > \varepsilon_0\}. \tag{12}$$

Meanwhile, the ascending delay vector $\boldsymbol{\tau} = [\tau_1, \tau_2, \ldots, \tau_{P_1P_2}]$ is recorded at the BS for all paths.

### *B. Angle Estimation at UE and BS*

The angle information at the BS and UE is obtained by utilizing specific subcarriers for individual path estimation. Based on the RIS angle information $\mathbf{i}_R$, the reflection patterns for the second stage are determined as

$$\boldsymbol{\Phi}_{k_2} = \frac{M^D}{M}\widetilde{\mathbf{C}}_R^{\dagger}[b](:, [\mathbf{i}_R]_{k_2}), \tag{13}$$

where $k_2 = 1, 2, \ldots, P_1P_2$ denotes the path index. The design of $\boldsymbol{\Phi}_{k_2}$ in Eq. (13) ensures a single non-zero element in $\widetilde{\mathbf{C}}_R[b]\boldsymbol{\Phi}_{k_2}$, guaranteeing the existence of approximately only one path in the channel. By utilizing the reflection patterns $\boldsymbol{\Phi}_{k_2}$ and CS algorithms to estimate the sparse channel represented by Eq. (7), we obtain the angle information $\mathbf{i}_{B,u}$ of each path at the BS and UE as

$$[\mathbf{i}_{B,u}]_{k_2} = \underset{1\le i\le N_t^D N_r^D}{\arg\max}\ ([\widehat{\boldsymbol{\omega}}_{k_2}[b]]_i), \tag{14}$$

where $\widehat{\boldsymbol{\omega}}_{k_2}[b]$ is the sparse vector estimated by the CS algorithm using reflection pattern $\boldsymbol{\Phi}_{k_2}$ for the $b$-th subcarrier. The RIS is deployed close to the BS (Section II), such that the delay from the RIS to the BS can be neglected. Based on the delay information $\boldsymbol{\tau}$, we design the RIS switching time point $\boldsymbol{\kappa}$ for each path as

$$[\boldsymbol{\kappa}]_i = [\boldsymbol{\tau}]_i - \delta, \tag{15}$$

where $\delta$ is the minimum RIS switching time, satisfying $|\tau_i - \tau_j| > \delta$ for different path delays. In cases where the delay difference between $P_d$ paths is smaller than $\delta$, a total of $P_d$ OFDM symbols are required for distinguishing and estimating them. The RIS reflection pattern switching based on path delays is more pilot-efficient than traditional switching based on OFDM symbol intervals, as channels of multiple RIS reflection patterns corresponding to different paths are estimated within one OFDM symbol.

For non-line-of-sight (nLoS) paths, the delay $\tau_{k_2}$ of each path is assumed to follow a Rayleigh distribution [17]. For cases where $|\tau_i - \tau_j| > \delta$, the required estimation duration decreases from the $P_1P_2$ OFDM symbol time slots $P_1P_2\epsilon$ to one OFDM symbol time slot $\epsilon$. The pilot reduction rate $s_r$ is

$$s_r = 1 - \frac{1}{P_1P_2}. \tag{16}$$

For cases where the path delay difference can be less than $\delta$, according to the Rayleigh distribution, the probability $p_\tau(n = 2)$ of compact delays for two paths is

$$p_\tau(n=2) = \binom{P_1P_2}{2}\int_{-\delta}^{\delta}(R * R')(\Delta\tau)\,\mathrm{d}(\Delta\tau), \tag{17}$$

where $R(x) = \frac{x}{\sigma^2}e^{-\frac{x^2}{2\sigma^2}}$ is the Rayleigh distribution function, and $\sigma$ is the scale parameter chosen such that the cumulative probability is $1 - e^{-8}$. $\binom{n}{k} \triangleq \frac{n!}{k!(n-k)!}$ is the binomial coefficient, and $p_u \triangleq \int_{-\delta}^{\delta}(R*R')(\Delta\tau)d(\Delta\tau)$ is the probability that delay difference of two paths is less than the minimum RIS switching time. $(R * R')(\Delta\tau)$ denotes the convolution of the functions $R$ and $R'$, with $R'(x) = R(-x)$. The probability of compact delays for at least $l$ ($l \ge 2$) paths is

$$p_\tau(n=l) = \frac{\binom{P}{l}\prod_{i=1}^{\frac{l(l-1)}{2}}\left(\frac{P(P-1)}{2} - i + 1\right)p_u^{\frac{l(l-1)}{2}}}{\sum_{i=l}^{L}\binom{i(i-1)/2}{l(l-1)/2}\binom{P}{i}}, \tag{18}$$

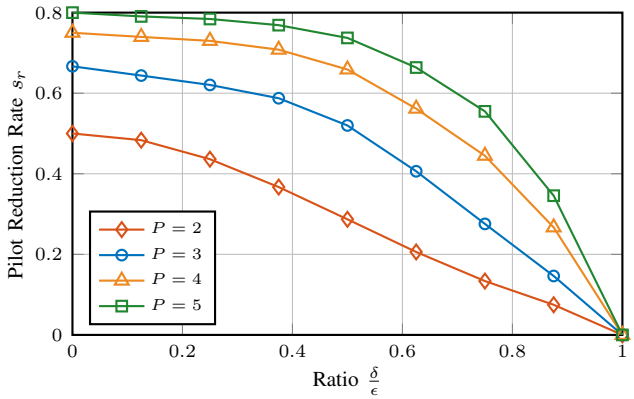


Fig. 2. Pilot efficiency gain in CE with the proposed method.

where $L \triangleq \min\{l(l-1), P\}$ and $P \triangleq P_1 P_2$. Therefore, Eq. (16) can be expanded to

$$s_r = 1 - \frac{1 + \sum_{i=2}^{P} p_r(n=i)}{P}. \tag{19}$$

Based on Eq. (19), Fig. 2 illustrates the gain in pilot efficiency (i.e., higher $s_r$), particularly when the minimum RIS switching time $\delta$ is smaller.

### C. Wideband Gain Estimation

In the third stage, the path gains corresponding to all subcarriers are estimated. The same reflection patterns $\mathbf{\Phi}_{k_2}$ from Section III-B are employed to estimate the paths one by one. With the obtained angle information $\mathbf{i}_{B,u}$, Eq. (7) can be reconstructed as

$$\widetilde{\mathbf{y}}_{k_2} = \widetilde{\mathbf{Q}}\widetilde{\boldsymbol{\omega}}_{k_2} + \widetilde{\mathbf{n}}_{k_2}, \tag{20}$$

where $\widetilde{\mathbf{y}}_{k_2} \in \mathbb{C}^{N_r^B N_t^B B \times 1}$, $\widetilde{\mathbf{n}}_{k_2} \in \mathbb{C}^{N_r^B N_t^B B \times 1}$, and $\widetilde{\mathbf{Q}} \in \mathbb{C}^{N_r^B N_t^B B \times B}$ are defined as

$$\begin{cases} \widetilde{\mathbf{y}}_{k_2} \triangleq [\mathbf{y}_{k_2}[1]^{\mathsf{T}}, \ldots, \mathbf{y}_{k_2}[B]^{\mathsf{T}}]^{\mathsf{T}}, \\ \widetilde{\mathbf{n}}_{k_2} \triangleq [\mathbf{n}_{k_2}[1]^{\mathsf{T}}, \ldots, \mathbf{n}_{k_2}[B]^{\mathsf{T}}]^{\mathsf{T}}, \\ \widetilde{\mathbf{Q}} \triangleq \operatorname{diag}(\mathbf{q}[1], \ldots, \mathbf{q}[B]), \end{cases} \tag{21}$$

where $\mathbf{q}[b]$ is the $[\mathbf{i}_{B,u}]_{k_2}$-th column of $\mathbf{Q}[b]$, arranged into $\widetilde{\mathbf{Q}}$ by block diagonalization and $\mathbf{Q}[b] \triangleq \mathbf{P}(\mathbf{D}_u^*[b] \otimes \mathbf{D}_B[b])$. Hence, $\widetilde{\boldsymbol{\omega}}_{k_2} \in \mathbb{C}^{B\times 1}$ contains the path gains and delay information for all $B$ subcarriers corresponding to the $k_2$-th path. Subsequently, the least squares (LS) algorithm [18] can estimate $\widetilde{\boldsymbol{\omega}}_{k_2}$, and the sparse channel vector $\boldsymbol{\omega}_{k_2}[b]$ for the $b$-th subcarrier corresponding to the $k_2$-th path is obtained as

$$[\boldsymbol{\omega}_{k_2}[b]]_i = \begin{cases} [\widetilde{\boldsymbol{\omega}}_{k_2}]_b, & i = [\mathbf{i}_{B,u}]_{k_2}, \\ 0, & \text{otherwise}. \end{cases} \tag{22}$$

Based on Eq. (22), the channel $\mathbf{H}_{k_2}[b]$ corresponding to the $k_2$-th path for $b$-th subcarrier can be represented as

$$\mathbf{H}_{k_2}[b] = \operatorname{vec}_{N_r,N_t}^{-1}(\mathbf{D}_u^*[b] \otimes \mathbf{D}_B[b])\boldsymbol{\omega}_{k_2}[b], \tag{23}$$

where $\operatorname{vec}_{N_r,N_t}^{-1}(\mathbf{a})$ denotes reshaping vector $\mathbf{a}$ into an $N_r \times N_t$ matrix. Therefore, the channel $\mathbf{H}[b]$ for the $b$-th subcarrier is

$$\mathbf{H}[b] = \sum_{k_2=1}^{P_1 P_2} \gamma_{k_2} \mathbf{H}_{k_2}[b], \tag{24}$$

where $\gamma_{k_2} \triangleq \widetilde{\mathbf{C}}_R[b]([\mathbf{i}_R]_{k_2}, :)\mathbf{\Phi}$.

### D. Complexity and Pilot Overhead Analysis

To show the efficiency of our proposed scheme, we compare both computational complexity and pilot overhead with the state-of-the-art schemes.

The computational complexity and pilot overhead comparisons are presented in Table I, where $P = P_1 P_2$, $P$ and $P'$ are the sparsity of $\mathbf{s}_k[b]$ and $\boldsymbol{\omega}_k[b]$. $K_1$ represents the number of reflection patterns utilized for angle acquisition at the RIS. $Q$ and $Q'$ are the average pilot overheads for each $\mathbf{\Phi}_k$ to the block sparse channel formulation [12] and Eq. (7). With OMP [4] employed for the second stages, and the LS algorithm utilized for the third stage, the overall computational complexity is comprised of three stages. The complexity of the first stage is 0, as it only involves determining whether a signal is received to obtain angle information at the RIS. $\mathcal{O}(P_1 P_2 Q_2 N_r^G N_t^G)$ is the computational complexity of the second stage and $\mathcal{O}(P_1 P_2 Q_3 B N_r^B N_t^B)$ is for the third stage, where $Q_2$ and $Q_3$ are the average pilot overheads for each reflection pattern in the second and third stages, respectively. As for the pilot overhead, due to the excessive high dimensionality incurred by directly constructing a block sparse vector based on Eq. (6), $Q_1 < Q_3 < Q_2 = Q' \ll Q$. Besides, $P' < P < K_1 \ll \min\{M^D, B\}$, since the terahertz channels exhibit strong sparsity and the wide bandwidth characteristics. Overall, our proposed CE framework offers lower complexity and fewer pilot overheads than existing works.

TABLE I
COMPLEXITY AND PILOT OVERHEAD COMPARISONS

| CE Method | Complexity | Pilot Overhead |
|---|---|---|
| Eq. (6) [12] | $\mathcal{O}(PQM^D N_r^D N_t^D)$ | $Q$ |
| Eq. (7) [7] | $\mathcal{O}(P'Q'M^D B N_r^D N_t^D)$ | $M^D B Q'$ |
| Proposed | $\mathcal{O}(PQ_2 N_r^G N_t^G + PQ_3 B N_r^B N_t^B)$ | $K_1 Q_1 + PQ_2 + PBQ_3$ |

[1] $P' < P < K_1 \ll \min\{B, M^D\}$;
[2] $N_r^B N_t^B \ll \min\{N_t N_r, M^D\}$;
[3] $Q_1 < Q_3 < Q_2 = Q' \ll Q$.

## IV. Simulation Results

Fig. 3 presents a comparative analysis between our proposed method and existing research, as referenced by [7] and [12]. The work by [7] employs Eq. (7) to estimate $M^D$ reflection patterns, while [12] utilizes the property of shared support among different subcarriers and adopts BOMP to reconstruct Eq. (6). Performance evaluation is based on the normalized mean square error (NMSE) to assess the CE accuracy, with the Oracle LS method providing a lower bound by assuming perfect angle knowledge.

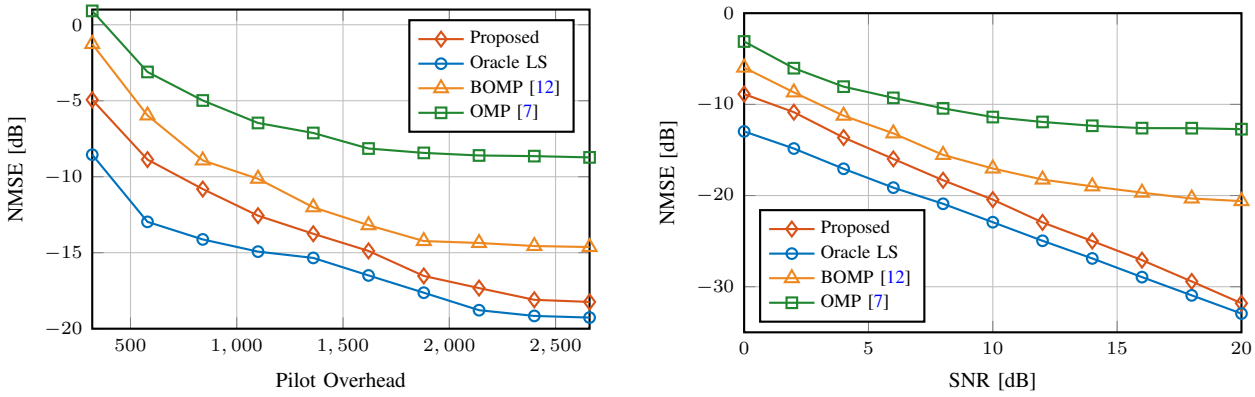


(a) NMSE v.s. pilot overhead with SNR $= 0$ dB.

(b) NMSE v.s. SNR with pilot overhead as 580.

Fig. 3. Simulation results with $P_1 = P_2 = 2$, $M = M^D = M_x \times M_y = M_x^D \times M_y^D = 8 \times 8$, $N_r^B = N_t^B = 2$, $N_t^D = N_t = 8$, $N_r^D = N_r = 16$, number of subcarriers $B = 64$.

In Fig. 3(a), the proposed method achieves about 60% reduction in pilot overhead compared to [7] and more than 35% reduction compared to [12] while maintaining an NMSE of $-5$ dB. In Fig. 3(b), our method consistently outperforms [12] and [7], with gains of 3 dB and 5 dB respectively in the SNR range from 0 dB to 10 dB. Moreover, our method exhibits no error floor, achieving gains of 10 dB and 18 dB at SNR $= 20$ dB.

## V. Conclusion

In this paper, we propose a high temporal efficiency local subdivisional CE method for RIS-assisted THz MIMO-OFDM systems. Our simulation results underscore the efficacy of this approach, revealing a remarkable reduction of pilot overhead while maintaining comparable levels of channel estimation accuracy. In addition, future work can explore the integration of more realistic models, further enhancing the applicability and robustness of the proposed method in real-world scenarios.

## References


[1] K. Rikkinen, P. Kyosti, M. E. Leinonen, M. Berg, and A. Parssinen, "THz radio communication: Link budget analysis toward 6G," *IEEE Commun. Mag.*, vol. 58, no. 11, pp. 22–27, Nov. 2020.

[2] H. Sarieddeen, M.-S. Alouini, and T. Y. Al-Naffouri, "An overview of signal processing techniques for terahertz communications," *Proc. IEEE*, vol. 109, no. 10, pp. 1628–1665, Oct. 2021.

[3] Z. Wan, Z. Gao, F. Gao, M. Di Renzo, and M.-S. Alouini, "Terahertz massive MIMO with holographic reconfigurable intelligent surfaces," *IEEE Trans. Commun.*, vol. 69, no. 7, pp. 4732–4750, Jul. 2021.

[4] J. Lee, G.-T. Gil, and Y. H. Lee, "Channel estimation via orthogonal matching pursuit for hybrid MIMO systems in millimeter wave communications," *IEEE Trans. Commun.*, vol. 64, no. 6, pp. 2370–2386, Jun. 2016.

[5] W. Zhao, C. Li, Z. Ji, Z. Guo, X. Chen, Y. You *et al.*, "Flexible high-level synthesis library for linear transformations," *IEEE Trans. Circuits Syst. II*, 2024, to be published, doi: 10.1109/TCSII.2024.3366282.

[6] C. Wei, Z. Yang, J. Dang, P. Li, H. Wang, and X. Yu, "Accurate wideband channel estimation for THz massive MIMO systems," *IEEE Commun. Lett.*, vol. 27, no. 1, pp. 293–297, Jan. 2023.

[7] Y. You, W. Zhao, L. Zhang, X. You, and C. Zhang, "Beam pattern and reflection pattern design for channel estimation in RIS-assisted mmwave MIMO systems," *IEEE Trans. Veh. Technol.*, pp. 1–5, 2024, to be published, doi: 10.1109/TVT.2023.3309950.

[8] A. Garg, S. Srivastava, N. Yadav, A. K. Jagannatham, and L. Hanzo, "Angularly sparse channel estimation in dual-wideband tera-hertz (THz) hybrid MIMO systems relying on Bayesian learning," *IEEE Trans. Commun.*, pp. 1–17, 2024, to be published, doi: 10.1109/TCOMM.2024.3367751.

[9] A. Brighente, M. Cerutti, M. Nicoli, S. Tomasin, and U. Spagnolini, "Estimation of wideband dynamic mmWave and THz channels for 5G systems and beyond," *IEEE J. Sel. Areas Commun.*, vol. 38, no. 9, pp. 2026–2040, Sep. 2020.

[10] X. Xu, S. Zhang, F. Gao, and J. Wang, "Sparse Bayesian learning based channel extrapolation for RIS assisted MIMO-OFDM," *IEEE Trans. Commun.*, vol. 70, no. 8, pp. 5498–5513, Aug. 2022.

[11] W. Zhao, Y. You, L. Zhang, X. You, and C. Zhang, "OMPL-SBL algorithm for intelligent reflecting surface-aided mmWave channel estimation," *IEEE Trans. Veh. Technol.*, vol. 72, no. 11, pp. 15 121–15 126, Nov. 2023.

[12] J. Wu, S. Kim, and B. Shim, "Parametric sparse channel estimation for RIS-assisted terahertz systems," *IEEE Trans. Commun.*, vol. 71, no. 9, pp. 5503–5518, Sep. 2023.

[13] J. Rodriguez-Fernandez and N. Gonzalez-Prelcic, "Channel estimation for frequency-selective mmWave MIMO systems with beam-squint," in *Proc. IEEE Global Commun. Conf. (GLOBECOM)*, Abu Dhabi, United Arab Emirates, Dec. 2018, pp. 1–6.

[14] K. Dovelos, M. Matthaiou, H. Q. Ngo, and B. Bellalta, "Channel estimation and hybrid combining for wideband terahertz massive MIMO systems," *IEEE J. Sel. Areas Commun.*, vol. 39, no. 6, pp. 1604–1620, Jun. 2021.

[15] Z. Kang, C. You, and R. Zhang, "IRS-aided wireless relaying: Deployment strategy and capacity scaling," *IEEE Wireless Commun. Lett.*, vol. 11, no. 2, pp. 215–219, Feb. 2022.

[16] P. Wang, J. Fang, H. Duan, and H. Li, "Compressed channel estimation for intelligent reflecting surface-assisted millimeter wave systems," *IEEE Signal Process. Lett.*, vol. 27, pp. 905–909, May 2020.

[17] Y. Li, N. Li, and C. Han, "Ray-tracing simulation and hybrid channel modeling for low-terahertz UAV communications," in *Prof. IEEE Int. Conf. Commun. (ICC)*, Montreal, QC, Canada, Jun. 2021, pp. 1–6.

[18] E. Karami, "Tracking performance of least squares MIMO channel estimation algorithm," *IEEE Trans. Commun.*, vol. 55, no. 11, pp. 2201–2209, Nov. 2007.